Optoacoustic Mesoscopy Analysis and Quantitative Estimation of Specific Imaging Metrics in Fitzpatrick skin phototypes II to V

Xiuting Li[1, †], Dinish U. S[1, †], Juan Aguirre[2, †], Renzhe Bi[1], Kapil Dev[1], Amalina Binte Ebrahim Attia[1], Suhanyaa Nitkunanantharajah[2], Lim Hann Qian[1], Mathias Schwarz[3], Yik Weng Yew[4], Steven Thng Tien Guan[4], Vasilis Ntziachristos[2, 5, *], Malini Olivo[1, *]

[†]Authors contributed equally

*Corresponding Author: E-mail: v.ntziachristos@helmholtz-muenchen.de; Malini_olivo@sbic.a-star.edu.sg;

[1] Laboratory of Bio-Optical Imaging, Singapore Bioimaging Consortium, Agency for Science Technology and Research (A*STAR), Singapore
[2] Munich School of Bioengineering, Technische Universität München, Germany
[3] iThera Medical GmbH, Munich, Germany
[4] National Skin Centre, Singapore
[5] Helmholtz Zentrum München, Institute for Biological and Medical Imaging, Germany

Keywords: Raster scanning optoacoustic mesoscopy, Fitzpatrick skin types, melanin signal intensity, total blood volume, vessel diameter

Short title: X. Li *et al.*: Optoacoustic mesoscopy analysis and quantitative estimation of specific imaging metrics in Fitzpatrick skin phototypes II to V

Raster Scanning Optoacoustic Mesoscopy (RSOM) is a novel optoacoustic imaging modality that offers non-invasive, label-free, high resolution (~7 μm axial, ~30 μm lateral) imaging up to 1-2 *mm* below the skin, providing novel quantitative insights into skin pathophysiology. As the RSOM image contrast mechanism is based on light absorption, it is expected that the amount of melanin present in the skin will affect RSOM images. However, the effect of skin tone in the performance of RSOM has not been addressed so far. Herein, we present the efficiency of RSOM for *in vivo* skin imaging of human subjects with Fitzpatrick (FP) skin types between II to V. RSOM images acquired from the volar forearms of the subjects were used to derive metrics used in RSOM studies, like total blood volume, vessel diameter, and melanin signal intensity. Our study shows that the melanin signal intensity derived from the RSOM images exhibited an excellent correlation with that obtained from a clinical colorimeter for the subjects of varying FP skin types. We could successfully estimate the

This article has been accepted for publication and undergone full peer review but has not been through the copyediting, typesetting, pagination and proofreading process, which may lead to differences between this version and the Version of Record. Please cite this article as doi: 10.1002/jbio.201800442

vessel diameter at different depths of the dermis. Furthermore, our study shows that there is a need to compensate for total blood volume calculated for subjects with higher FP skin types due to the lower signal-to-noise ratio in dermis, owing to strong absorption of light by melanin. This study sheds light into how RSOM can be used for studying various skin conditions in populations with different skin phenotypes.

1. Introduction

Optoacoustic imaging is based on the detection of ultrasound waves generated within tissue in response to pulsed light illumination [1]–[3]. The light-absorbing molecules absorb the pulsed light depositing heat in tissue which leads to thermo-elastic expansion. This expansion produces ultrasound waves, which are detected by transducers. Reconstruction algorithms are used to convert wave-front information into a three-dimensional (3D) map of the absorbed light. Optoacoustic technique generates images based on optical contrast at depths up to few centimetres with the spatial resolution of ultrasound technique. The resolution of traditional optical imaging techniques is drastically degraded after a few hundred microns depth due to strong light scattering, while ultrasound waves are barely affected by scattering when travelling through tissue[4]–[8], allowing resolutions of 200 μm, at centimetres depth. Optoacoustic imaging has played an increasingly predominant role in fundamental biological research and clinical practice due to its scalability and unique optical absorption contrast. It can image at various system levels and provide anatomical, functional, molecular and fluid-dynamic information[9], [10]. Raster-scan optoacoustic mesoscopy (RSOM) is a novel optoacoustic imaging technique that offers non-invasive, label-free, high resolution (7-30 μm, axial and lateral) images and it is well suited for skin imaging applications. Its penetration depth is “mesoscopic”[11], meaning that it images at few millimetres depth while largely preserving its high-resolution capabilities.

To perform RSOM imaging, a spherically focused transducer is scanned together with illumination fiber bundles over a region of interest. The optoacoustic waves generated in the tissue in response to pulsed laser illumination are collected. Data is tomographically reconstructed to yield an image that represents the 3D distribution of absorbed light within the skin. When using Nd:Yag lasers for illumination at 532 nm wavelength, RSOM can image below the skin surface up to 1-2 *mm*. The reconstructed images show the distribution of melanin and haemoglobin in the epidermis and dermis, providing detailed views of the skin microvascular system at a ~7 μm axial resolution and ~30 μm lateral resolution. RSOM has been successfully used for proof-of-concept imaging of skin inflammatory conditions, such as psoriasis and atopic eczema[12]. In these studies, skin-specific metrics, such as total blood volume (TBV) and thickness of the epidermis, have been proposed for evaluating cutaneous inflammation which showed stark contrast between psoriasis and control conditions[12]. However, previous RSOM studies have been performed in populations with light skin phenotypes[13]–[16]. Since RSOM contrast generation is based on light absorption, it is mandatory to study its performance in darker skin phenotypes as well as to understand the possible implications in its clinical translation.

Our skin and hair colour is determined by melanin which gives us innate protection against ultraviolet light. Melanin production initiates in the basal level of the epidermis, being stimulated by ultraviolet light. Fitzpatrick (FP) skin phototype is used as a surrogate to describe different skin colour tones or skin pigmentation and photo-sensitivities. It comprises of six types (I through VI) and skin typed based on patient-reported sensitivity and reactivity to ultraviolet light and tanning response. Type I skin type is the fairest, and most susceptible to photo or laser-induced damage while the most resistant to tanning. Type VI on the other hand do not burn and likely to tan upon sun exposure.

Herein, we conducted a pilot *in vivo* skin imaging using RSOM in 18 healthy human subjects with FP skin types varying between II to V. We investigate the effect of skin phototype in deducing various RSOM-based metrics from the images taken at the volar forearms of the subjects. This can further help in understanding the efficiency of RSOM for studying various skin disorders in populations with different skin phenotypes.

2. Methodology

2.1. Subjects

A total of 18 volunteers of FP skin types II (n = 3), III (n = 7), IV (n = 4) and V (n = 4) were included in this study and imaged following approval by Domain Specific Review Board (DSRB) of National Health Group, Singapore (2017/00932).

2.2. RSOM system

Figure 1 shows the RSOM Explorer C50 system (iThera Medical GmbH, Germany) used in this study. A diode-pumped solid state (DPSS, Nd:YAG) laser is used, providing < 1 *ns* pulses and a per-pulse energy of up to 125 μJ on the sample surface. The light spot scanned over the region of interest measures approximately 5 *mm* x 3 *mm*. The light fluence during the scanning was simulated and the pulse repetition rate was adjusted such that the maximum light fluence was always below the maximum permissible exposure limit of 20 mJ/cm^2 per pulse and 200 mW/cm^2 average power. The repetition rate of the laser was 270 *Hz*. An in-tandem illumination-detector raster-scans the 2D skin region of interest (ROI) on a regularly-spaced acquisition grid[17]. An articulated arm allows the flexibility of mesoscope scanning head for positioning the scan of patients' correct ROI, situated in the lower arm. The acquisition time is about 2 mins. 3D images were obtained using a beam forming algorithm that assumes that a point detector is located at the focal point of the transducer, and that the

detector accepts signals only within a cone that has an opening angle defined by the numerical aperture of the transducer.

2.3. Imaging process

The processing of acquired RSOM images was carried out in four stages; (1) pre-processing of the acquired data, (2) the 3D beam-forming reconstruction algorithm, (3) post-processing of reconstructed images and (4) calculating and analysis of specific imaging metrics. The first stage of pre-processing involved the filtering of reflection lines in the Fourier space, bandpass-filtering of the raw data, and automatic co-registration of the raw data[18], [19]. The second stage of reconstruction was based on beam forming algorithm[20]–[22]executed on a GPU to expedite for the reconstruction of 3D images in parallel. Some hollow parts might appear in the vessels if data acquisition was instantaneous and therefore the reconstruction would represent the haemoglobin distribution at a precise time point and hollow parts would appear in the smallest vessels. Since in our case, the acquisition times is ~ 2 min, the reconstructed images roughly represents the average of several images taken at different time points and therefore the microvascular tree can be observed without hollow parts. The third stage is incorporated with the motion correction and skin surface flattening to enhance the image quality [23]. The ultra-wide detection bandwidth was divided into two sub-bands, 11–33 *MHz* (low, red) and 33–99 *MHz* (high, green) for the concurrent visualization of big and small structures respectively in one image to prevent the masking of high frequencies by low frequencies. The motion correction algorithm was grounded on one assumption: the skin surface is taken to be continuous and smooth on a mesoscopic scale. Using a developed software algorithm, the skin surface was identified by the highly absorbing melanin layer in the epidermis such that the calculated skin surface was shifted to a flatten the surface for further analysis of vasculature features [23]. It is significantly

important to carry out the motion correction and skin flattening before any analysis to facilitate the segmentation of different skin layers.

The detailed methodologies employed for determining the specific imaging metrics are provided in the following subsections. Analysis of the differences of all FP skin types in each specific imaging metric was carried out by using one-way analysis of variance (ANOVA), which is a statistical test to assess the relative size of variance among the means of all FP skin types, giving an overall p value of significance of at least one group from the other groups.

2.3.1. Specific Imaging Metrics

We computed (1) the melanin signal intensity, (2) the signal to noise ratio (SNR) in the epidermis and dermis, (3) the total blood volume (TBV) in the dermis, and (4) the diameter of the blood vessels in both superficial and deep dermis.

2.3.2. Signal to noise (SNR)

We selected the signal from upper part of the dermis and epidermis, while noise is selected in a region right above the epidermis. For every measurement we double checked that no artefacts were present in the selected regions, which are due to reflection of sound at the lens interfaces in the transducer. The SNR in imaging was numerically defined as the ratio of the mean signal value (μ_{signal}) to the standard deviation (σ_{noise}) of background noise. The measurement of SNR for different FP skin types signifies the comparison between desired signal, *i.e.* highly resolved vasculature below skin with respect to the imaging noise. In the RSOM 3D image stack (500×250×150) recorded for subjects with different FP skin type, the SNR was calculated in both epidermis and dermis area. First, to calculate the mean of signal in 3D RSOM stack, the signal must be separated from the noise. A threshold was chosen for different FP skin type to separate the signal from the background noise in each 3D RSOM image stack. In this RSOM x-z scan (a 500×250 2D image) of the 3D stack, the thickness and

width of the epidermis and dermis layer was chosen to be ~ 20×200 pixels and ~ 200×200 pixels respectively to calculate the mean of signal in the area. Next, a standard deviation of imaging noise was calculated in the 100×200 pixels area above the skin surface with in same RSOM image but without threshold removal to accommodate the background noise. The same process was repeated for all the 150 2D images in the stack. Finally, the average of these values was calculated over 150 2D image stack and the SNR was calculated.

2.3.3. Melanin signal intensity

After the skin surface was flattened, the 3D RSOM stack is ready for layer segmentation. Considering the thickness of melanin layer, epidermis and dermis are relatively consistent across the entire imaging region, we averaged all pixels in x-y plane along the depth (z-axis). Therefore, two plots of low-frequency channel and high-frequency channel along z-axis were generated, i.e. the RSOM optoacoustic profile along the skin depth. Since melanin is in the basal layer of the epidermis, which absorbs 532 nm light strongly, there is an overlap of the first dominant peak between these two profiles. Based on the pixel location of the intensity peak overlap, the center of melanin layer could be registered. The full width at half maximum (FWHM) of the first dominant intensity peak from low-frequency band of RSOM optoacoustic profile along the depth direction was taken as the thickness of the melanin layer. We take the RSOM signal intensity in this melanin layer as ‘melanin signal intensity’ in our analysis.

2.3.4. Total blood volume

We calculated the TBV based on image segmentation, in which we apply a threshold to the dermal region of RSOM 3D image stack to obtain a binary mask. We set the voxels to be 1 when its value is above the threshold, and the rest of voxels to be 0. The TBV was taken as the count the total number of voxels with value of one in the segmented dermis. The selection

of threshold should be based on the SNR of each FP skin type group. We chose 20% to 25% of the maximum voxel value as the threshold for FP skin type II, and increased accordingly as higher FP skin type, due to the lower SNR values in dermis of higher FP skin type. The TBV was then calculated as TBV = $\sum N \times dV$, where N is the number of voxels with value of one in the certain voxel volume dV. Based on the above description of SNR, we have applied increasing threshold as the FP skin type increases to segment the vasculature as a compensation to the lower SNR values in dermis of higher FP skin types.

2.3.5. Vessels diameter

The diameters of deep and superficial vessels in dermis were measured from the RSOM x-z or y-z 2D images, which are the maximum intensity projection of the RSOM 3D image stack along the depth direction, called RSOM cross-sectional images, obtained from each FP skin type group. The selection of the blood vessels should be parallel to the skin surface as much as possible, and in the same depth in dermis from different FP skin type group, while the optoacoustic profile should be perpendicular to the chosen blood vessels. The FWHM of the optoacoustic signal in the RSOM cross-sectional images was calculated as the vessel diameter.

2.3.6. Clinical colorimeter

A colorimeter is a light-sensitive device used for measuring the intensity or concentration of the colour. It is widely used in clinical trials as it is easy to use, time-saving, and can provide reliable and accurate results. In our study, we used the M value and ITA (individual typology angle) value of clinical colorimeter (Delfin Skin Color Catch) data. As a standard to describe the density of melanin in the skin layer, M index indicates the melanin in skin pigmentation. The ITA value is used to describe the different FP skin types i.e. the higher the ITA value, the lighter the skin.

3. Results and Discussion

3.1. RSOM cross-sectional images

The RSOM cross-sectional images for subjects from different FP skin types revealed marked differences as shown in Figure 2a, in which the low and high frequency components are labelled in red and green colour respectively. All scale bars are 500 μm. The representative skin type from different FP skin types is shown in Figure 2b, whereby the scanned ROI was in the centre of the volar forearms. We selected the volar forearm region to avoid the interference from hair, which is dominant in Asian skin. Due to the high melanin content in hair, it might reduce the image quality and hence limit the penetration to achieve sufficient vasculature information in dermis. This problem can be solved by shaving the target area before imaging. The influence of the sub-epidermal part of the hair shaft is minimal and RSOM could provide nice images of the hair shafts and bulb. Only a small percentage of the hair length is found beneath the skin surface and hence the influence will be minimum. In Figure 2a, the different layers of the skin can be observed; the uppermost layer is the epidermis (E), followed by the dermis (D) after surface flattening. From the epidermis, only the melanin layer is observed. The melanin layer may have in homogeneities and even hollow parts. In the latter case, the skin surface detection algorithm tends to provide interpolated values from the boundaries of the hollow areas. Our aim is to separate melanin from haemoglobin when performing the maximum intensity projections in order to separately visualize the microvascular structures from the melanin structures. The cutaneous blood vascular architecture consists of a lower and an upper horizontal plexus. The capillary loops (CL) extends from the former and can be seen from the ‘dot’-like structures in the image

while the bigger vascular plexus (VP) forms the lower horizontal plexus. Notably, bigger vessels (lower frequency band) appear red in colour while smaller structures (higher frequency band) appear green. The overlap between the red and green signals (giving yellow signals) was taken as the melanin layer, in accordance with the calculation of the melanin signal intensity.

As the FP skin type increases, we can observe that the melanin signal intensity is appreciably increasing, while the blood vessels in the deep plexus are barely seen in higher FP type IV and V. This is because the melanin absorbs the most of incident light, which can't effectively penetrate the deeper vascular structure region in higher FP skin types. The clinical ITA value for subjects with different FP skin types is shown in Figure 2c. The subjects with higher FP skin types (IV and V) exhibited lower ITA value.

3.2. Signal to noise vs FP skin types

For SNR calculation, regions selected for the signal and noise are shown in Figure 3a. The SNR ratios calculated for subjects with different FP skin type in the epidermis and dermis are shown in Figure 3b and 3c. It is evident from these plots that the subjects with high FP skin types (IV and V) exhibited high SNR in the epidermis as the light is not able to penetrate deeper into the skin due to presence of high melanin signal intensity. Similarly, the SNR is higher within the dermis for the low FP skin type subjects as the incident light could penetrate deeper into skin and allow high resolution vasculature imaging in the dermis. The low SNR in dermis for higher FP skin type can be attributed to the low mean signal value; whereas the standard deviation of background noise value remains similar to other FP skin type cases. Due to the relatively low SNR in dermis for high FP skin type subjects, there exists a limitation of the RSOM imaging system that restricts it for deep vascular imaging for subjects with higher skin pigmentation. The SNR is depth-dependent due to both signal attenuation and ultrasound detector sensitivity. However, the fact that several artefacts are

present in the image that makes it difficult to have an automatic calculation of depth dependent SNR. The use of depth dependant SNR is beyond the scope of this paper.

3.3 Melanin signal intensity vs clinical colorimeter data

The RSOM optoacoustic profiles along the skin depth in low-frequency band and high-frequency band are shown in Figure 3d (image of a representative FP type III) in red and green signals respectively. The overlap of the first dominant peak between two profiles is taken as the melanin layer, which is corresponding to the yellow part of the RSOM cross-sectional images in Figure 2a. The thickness of melanin layer is calculated as the FWHM of the overlap of the first dominant peak between these two profiles, denoted as blue cross line. As shown in Figure 3e, melanin signal intensity acquired from RSOM images shows good correlation with the melanin index (M) from clinical colorimeter measurements (r = 0.8615) and of significant difference $p < 0.0001$ from one-way ANOVA indicates a robust linear trend. Colorimetry provides values that represent the perception of skin color. It is not the aim of this paper to derive the melanin concentration from the melanin signal intensity. Obtaining absolute concentration values from optoacoustic signals is a challenging task due to the complex relationship between the absorption coefficient and the light fluence[24]. Our results indicate that the melanin intensity signal correlates well with our perception of skin tone.

3.4 Total blood volume vs FP skin types

TBV in the dermis calculated for subjects with different FP skin types is shown in Figure 3f. TBV decreased significantly as a function of FP skin type from II to V, in which the mean value of TBV in FP type II group is approximately 2 times of that of FP type IV group and 7 times of that of FP type V group. For TBV, $p < 0.05$ indicates a statistically significant difference across all FP skin types. As the subjects in each FP skin type group are healthy

volunteers, the vasculature volume in the dermis between subjects are assumed to be similar regardless of skin type. However, the observed decreasing trend of vasculature volume was due to the light absorbed by melanin of the higher FP skin types, even after applying a SNR dependent functional threshold to each FP skin type as a compensation. In this study, we are using an average SNR related TBV to study the quantitative abilities of RSOM between human groups with different FP scores. We are currently developing a more advanced depth dependent SNR rather than an average SNR metric and planning to implement it in our on-going clinical studies. The limitations of the RSOM is evident in the disparity of the TBV calculated in different FP skin types. It is implied that there is still a need to compensate for the measured TBV in the dermis for subjects with higher FP skin type due to lower SNR owing to strong melanin absorption and the melanin signal intensity can be used as a correction factor for the calculation of TBV in dermis. Another and simple solution to account for this disparity is to use FP classification, colorimetry value or the mean melanin signal intensity as calculated by RSOM as a co-variable when performing inter-subject RSOM analysis. Alternative strategies such as optimizing the choice of laser wavelength, development of multi-wavelength imaging system (MSOM), choice of optimal transducer frequency or improved algorithm for image processing are currently being investigated at different levels. Nevertheless, the influence of the FP score will be minimal when performing therapy monitoring studies or when analysing inflammatory diseases in which the melanin disappears from the affected skin areas like in the case of psoriasis.

3.5. Vessels diameter in deep and superficial dermis vs FP skin types

A representative image from group FP III together with the selected vessels' optoacoustic profiles denoted as blue lines in the superficial and deep dermis are shown in Figures 4a and 4c respectively. The measured mean diameters the two types of vessels in the dermis i.e. deep (~ 1 *mm* depth) and superficial vessels (80 μm depth) were shown in Figures 4b and 4d

respectively. No statistically significant differences were detected ($p > 0.05$) among the mean vessel diameters of all FP skin types in both deep and superficial dermis. Since the blood vessels in the deep plexus are barely seen in higher FP type IV and V, we segmented the dermis region to exclude the effect of their high melanin signal intensity in order to have a better vision of the blood vessels in the deep plexus to complete the calculation. Moreover, the calculated RSOM values of deep vessel diameter (~25-30 μm) and superficial vessel diameter (~15-20 μm) are in agreement with reported data for healthy subjects acquired by other optical methods[25]–[27]. Vessel diameter derived from similar RSOM imaging system was previously compared with histology and phantom data and it exhibited great correlation [12].

Herein, we demonstrate the efficiency of RSOM in the quantitative estimation of specific imaging metrics from FP skin type II to V in the human volar forearm. RSOM represents a non-invasive imaging method to estimate the relative melanin signal intensity of different skin phototypes. This is valuable in providing information on the individual's susceptibility to UV-induced disorders such as epidermal tumors; to predict an individual's risk of developing non-melanoma or melanoma skin cancers. Imaging the melanin distribution in the skin (chaotic vs regular) may present a novel option to monitor pigmentation disorders in the skin and their response to treatment. Furthermore, melanin signal intensity is useful in the evaluation of the UV protectors in the cosmetic industry. Moreover, dermal blood volume and blood vessel diameter were calculated from single wavelength RSOM images acquired at 532 nm. The ability to quantify cutaneous blood volume and vessel diameter also makes RSOM a potential tool in monitoring vascular disorders whereby prominent remodeling of the vasculature is involved. For example, vessel dilation has been reported in atopic dermatitis lesions[28]. By reconstructing the cutaneous vasculature via RSOM, therapy

monitoring of vascular disorders such as using lasers may prove useful for better disease management.

4. Conclusion

We successfully presented *in vivo* RSOM imaging of human subjects with FP skin types varying between II to V. RSOM images acquired from the lower volar arms of the healthy subjects were used to derive metrics such as SNR in both epidermis and dermis, melanin signal intensity in the skin layer, total blood volume in the dermis and vessel diameter in both superficial and deep vessels in the dermis. We found that the melanin signal intensity calculated from the RSOM images exhibited good correlation with the melanin index obtained from a standard colorimeter for the subjects across all FP skin types. RSOM imaging could also successfully estimate the vessel diameter in the dermis, which is in accordance with reported values. Our results showing TBV decreasing in the dermis of the control subjects as FP skin type increases, is attributed to the lower SNR in dermis owing to strong melanin absorption. RSOM imaging system has a limitation on the deep vascular imaging for the subjects with higher FP skin types. This necessitates the need to compensate for TBV measured by RSOM at higher FP skin types. The melanin signal intensity can be used as a correction factor for the calculation of TBV in dermis, by applying a SNR dependent functional threshold to each FP skin type. Alternatively, the melanin signal intensity or colorimetry values or FP scores can be used as co-variables for inter-subject RSOM studies. On the other hand, therapy monitoring studies will not be affected by skin phototypes. Moreover, in many inflammatory diseases the melanin layer disappears (e.g. psoriasis) and therefore, the imaging performance is not affected. This understanding is highly beneficial when translating RSOM as a clinical skin imaging modality, especially in subjects with higher FP skin types. We envision that this study will find potential clinical

application in estimating RSOM derived metrics for various skin inflammatory diseases such as psoriasis and atopic dermatitis, whereby vascular remodelling and acanthosis is observed.

Acknowledgements

Authors would like to thank Biomedical Research Council (BMRC), A*STAR, Singapore for the funding support.

References

[1] L. V. Wang, "Prospects of photoacoustic tomography," *Med. Phys.*, vol. 35, no. 12, pp. 5758–5767, 2008.
[2] L. Wang and S. Hu, "Photoacoustic Tomography: in Vivo Imaging Fro Organelles To Organs," *Science (80-.).*, vol. 335, no. 6075, pp. 1458–1462, 2012.
[3] J. Yao and L. V Wang, "Photoacoustic Microscopy," *Laser Phot. Rev*, vol. 7, no. 5, pp. 1–36, 2014.
[4] G. S. Sangha, N. J. Hale, and C. J. Goergen, "Adjustable photoacoustic tomography probe improves light delivery and image quality," *Photoacoustics*, vol. 12, no. July, pp. 6–13, 2018.
[5] J. Yao and L. V. Wang, "Sensitivity of photoacoustic microscopy," *Photoacoustics*, vol. 2, no. 2, pp. 87–101, 2014.
[6] L. V Wang, "Multiscale photoacoustic microscopy and computed tomography," *Nat. Photonics*, vol. 3, no. 9, p. 503, 2009.
[7] R. Bi *et al.*, "Photoacoustic microscopy for evaluating combretastatin A4 phosphate induced vascular disruption in orthotopic glioma," *J. Biophotonics*, no. February, pp. 1–7, 2018.
[8] S. J. Ford *et al.*, "Structural and Functional Analysis of Intact Hair Follicles and Pilosebaceous Units by Volumetric Multispectral Optoacoustic Tomography," *J. Invest. Dermatol.*, vol. 136, no. 4, pp. 753–761, 2016.
[9] J. Yao and L. V Wang, "Photoacoustics tomography: foundamentals, advances and prospect," *NIH Public Access*, vol. 6, no. 5, pp. 332–345, 2011.
[10] T. T. W. Wong *et al.*, "Label-free automated three-dimensional imaging of whole organs by microtomy-assisted photoacoustic microscopy," *Nat. Commun.*, vol. 8, no. 1, 2017.
[11] D. Razansky *et al.*, "Multispectral opto-acoustic tomography of deep-seated fluorescent proteins in vivo," *Nat. Photonics*, vol. 3, no. 7, p. 412, 2009.
[12] J. Aguirre *et al.*, "Precision assessment of label-free psoriasis biomarkers with ultra-broadband optoacoustic mesoscopy," *Nat. Biomed. Eng.*, vol. 1, no. 5, pp. 1–13, 2017.
[13] M. Schwarz, M. Omar, A. Buehler, J. Aguirre, and V. Ntziachristos, "Implications of ultrasound frequency in optoacoustic mesoscopy of the skin," *IEEE Trans. Med. Imaging*, vol. 34, no. 2, pp. 672–677, 2015.
[14] A. Berezhnoi, M. Schwarz, A. Buehler, S. V. Ovsepian, J. Aguirre, and V. Ntziachristos, "Assessing hyperthermia-induced vasodilation in human skin in vivo using optoacoustic mesoscopy," *J. Biophotonics*, no. November 2017, pp. 1–8, 2018.

[15] J. Aguirre *et al.*, "Assessing nailfold microvascular structure with ultra-wideband raster-scan optoacoustic mesoscopy," *Photoacoustics*, vol. 10, pp. 31–37, 2018.
[16] M. Kirillin, V. Perekatova, I. Turchin, and P. Subochev, "Fluence compensation in raster-scan optoacoustic angiography," *Photoacoustics*, vol. 8, pp. 59–67, 2017.
[17] M. Omar, M. Schwarz, D. Soliman, and P. Symvoulidis, "Pushing the Optical Imaging Limits of Cancer with Multi-Frequency- Band Raster-Scan Optoacoustic Mesoscopy (RSOM)," *NEO*, vol. 17, no. 2, pp. 208–214, 2015.
[18] A. Q. Bauer, R. E. Nothdurft, T. N. Erpelding, L. V. Wang, and J. P. Culver, "Quantitative photoacoustic imaging: correcting for heterogeneous light fluence distributions using diffuse optical tomography," *J. Biomed. Opt.*, vol. 16, no. 9, p. 096016, 2011.
[19] C. P. Favazza, O. Jassim, L. A. Cornelius, and L. V. Wang, "In vivo photoacoustic microscopy of human cutaneous microvasculature and a nevus," *J. Biomed. Opt.*, vol. 16, no. 1, p. 016015, 2011.
[20] D. S. Kermany *et al.*, "Identifying Medical Diagnoses and Treatable Diseases by Image-Based Deep Learning," *Cell*, vol. 172, no. 5, p. 1122–1124.e9, 2018.
[21] M. Xu and L. V. Wang, "Universal back-projection algorithm for photoacoustic computed tomography," *Phys. Rev. E - Stat. Nonlinear, Soft Matter Phys.*, vol. 71, no. 1, pp. 1–7, 2005.
[22] M. Schwarz, A. Buehler, J. Aguirre, and V. Ntziachristos, "Three-dimensional multispectral optoacoustic mesoscopy reveals melanin and blood oxygenation in human skin in vivo," *J. Biophotonics*, vol. 9, no. 1–2, pp. 55–60, 2016.
[23] M. Schwarz, N. Garzorz-Stark, K. Eyerich, J. Aguirre, and V. Ntziachristos, "Motion correction in optoacoustic mesoscopy," *Sci. Rep.*, vol. 7, no. 1, pp. 1–9, 2017.
[24] S. Tzoumas *et al.*, "Eigenspectra optoacoustic tomography achieves quantitative blood oxygenation imaging deep in tissues," *Nat. Commun.*, vol. 7, p. ncomms12121, 2016.
[25] I. M. Braverman, "The cutaneous microcirculation: Ultrastructure and microanatomical organization," *Microcirculation*, vol. 4, no. 3, pp. 329–340, 1997.
[26] I. M. Braverman and A. Keh-Yen, "Ultrastructure of the human dermal microcirculation. III. The vessels in the mid- and lower dermis and subcutaneous fat," *J. Invest. Dermatol.*, vol. 77, no. 3, pp. 297–304, 1981.
[27] I. M. Braverman and A. Yen, "Ultrastructure of the human dermal microcirculation: II. The capillary loops of the dermal papillae," *J. Invest. Dermatol.*, vol. 68, no. 1, pp. 44–52, 1977.
[28] Y. Zhang, H. Matsuo, and E. Morita, "Increased production of vascular endothelial growth factor in the lesions of atopic dermatitis," *Arch. Dermatol. Res.*, vol. 297, no. 9, pp. 425–429, 2006.

Figures

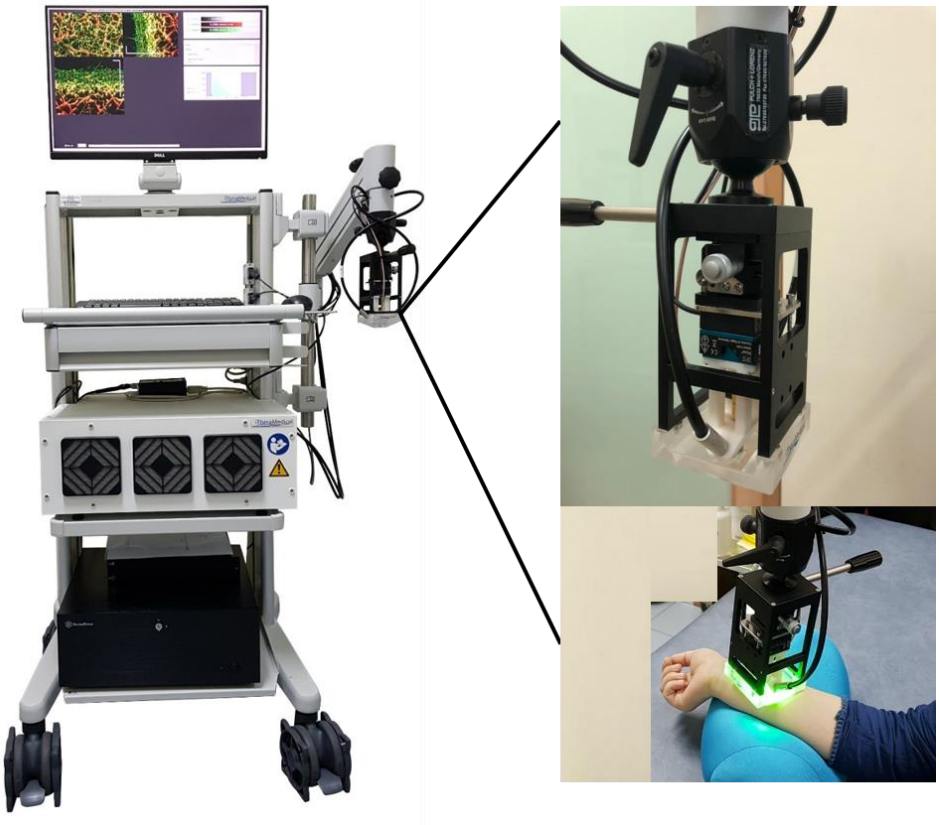

Figure 1. Image of the RSOM Explorer C50 system and the closer look of the scanning head in position, which is ready for image acquisition.

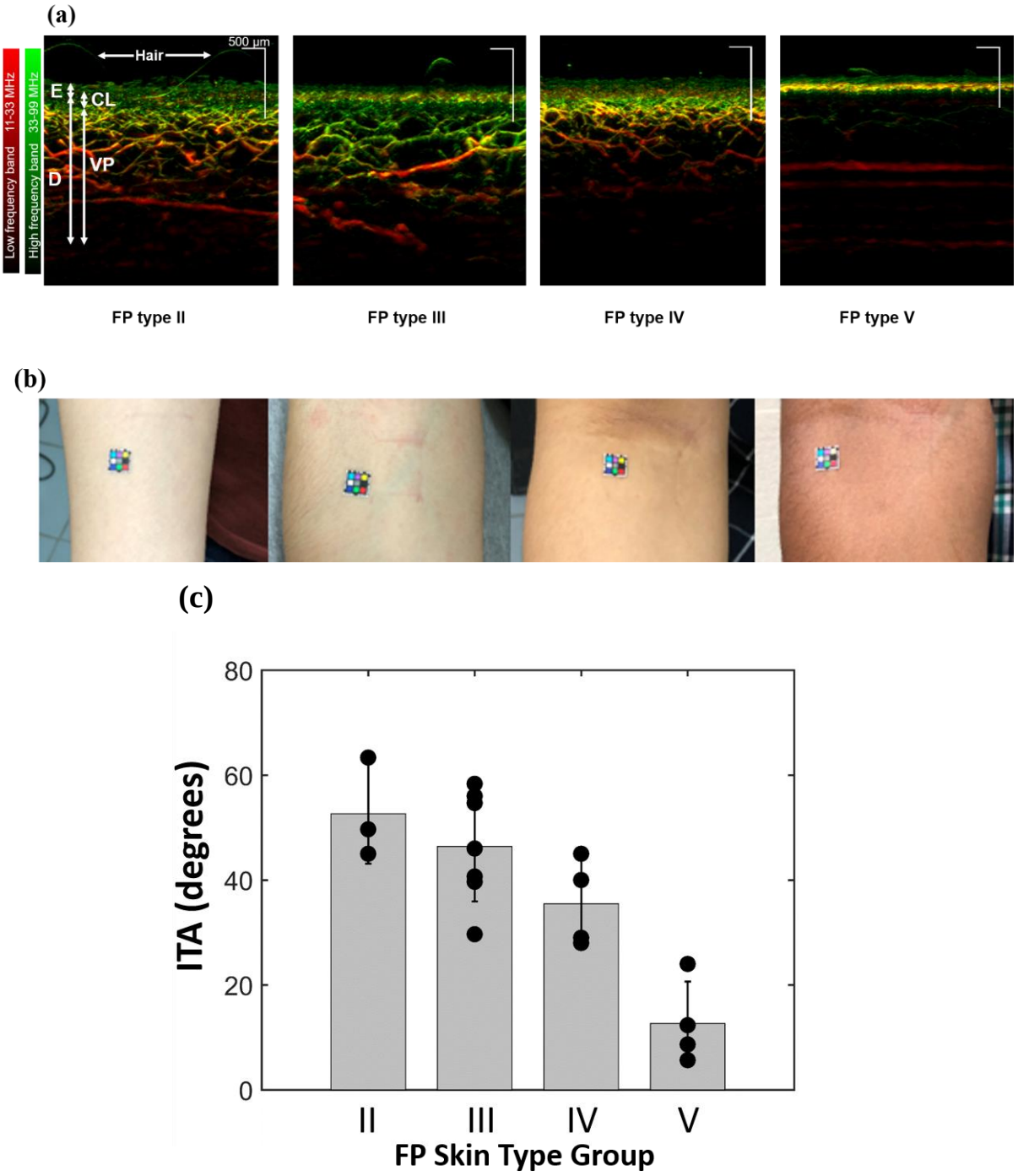

Figure 2. a) Representative RSOM images for each FP skin type indicating the different skin regions. The uppermost layer is the epidermis (E), followed by the dermis (D). The cutaneous blood vascular architecture consists of a lower and an upper horizontal plexus. The capillary loops (CL) extends from the former and can be seen from the 'dot'-like structures in the image while the bigger vascular plexus (VP) forms the lower horizontal plexus; **b)** Volar forearm region of the volunteers where RSOM images were acquired. All scale bars; 500 μm. A total of 18 volunteers of FP skin types II (n = 3), III (n = 7), IV (n = 4) and V (n = 4) were included; **c)** The average ITA value of the volunteers forearms for different FP skin types. The lower the ITA value, the darker the skin tone i.e. higher FP skin type.

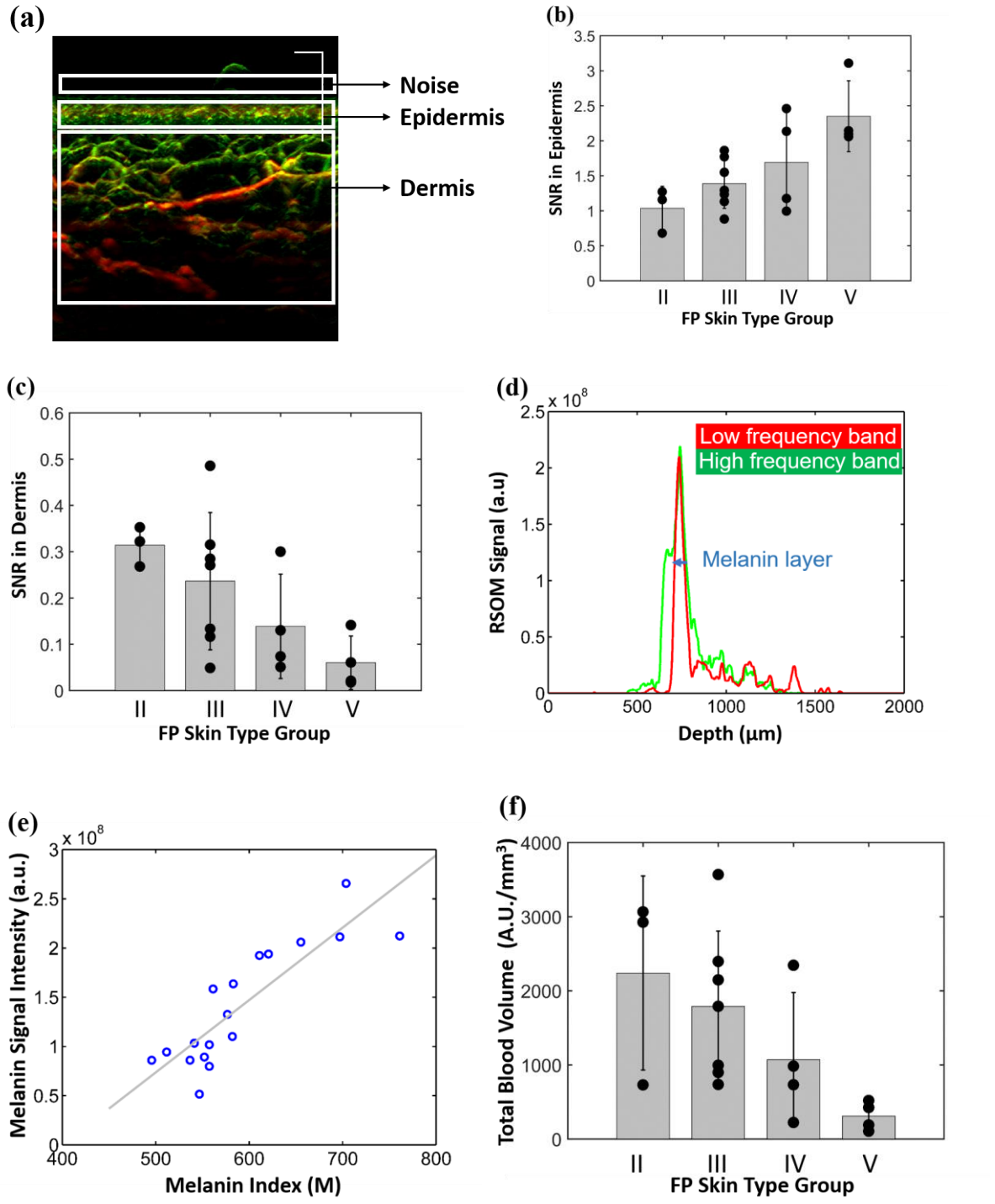

Figure 3. **a)** For SNR calculation, the noise and signal areas in epidermis and dermis are marked in one of the representative image of FP III; **b)** SNR in the epidermis and **c)** dermis skin regions for subjects with different FP skin; **d)** the RSOM optoacoustic profiles from the representative FP III image along the skin depth in low-frequency band (red) and high-frequency band (green), the thickness of melanin layer is calculated as the FWHM of the overlap of the first dominant peak between these two profiles, denoted as blue cross line; **e)** the correlation of the RSOM derived melanin signal intensity with the melanin index measured using a colorimeter from individual subjects across different FP skin types

(r = 0.8615; p < 0.0001); **f)** TBV in dermis for different FP skin types with p < 0.05 . TBV shows gradual decrease as a function of FP skin type.

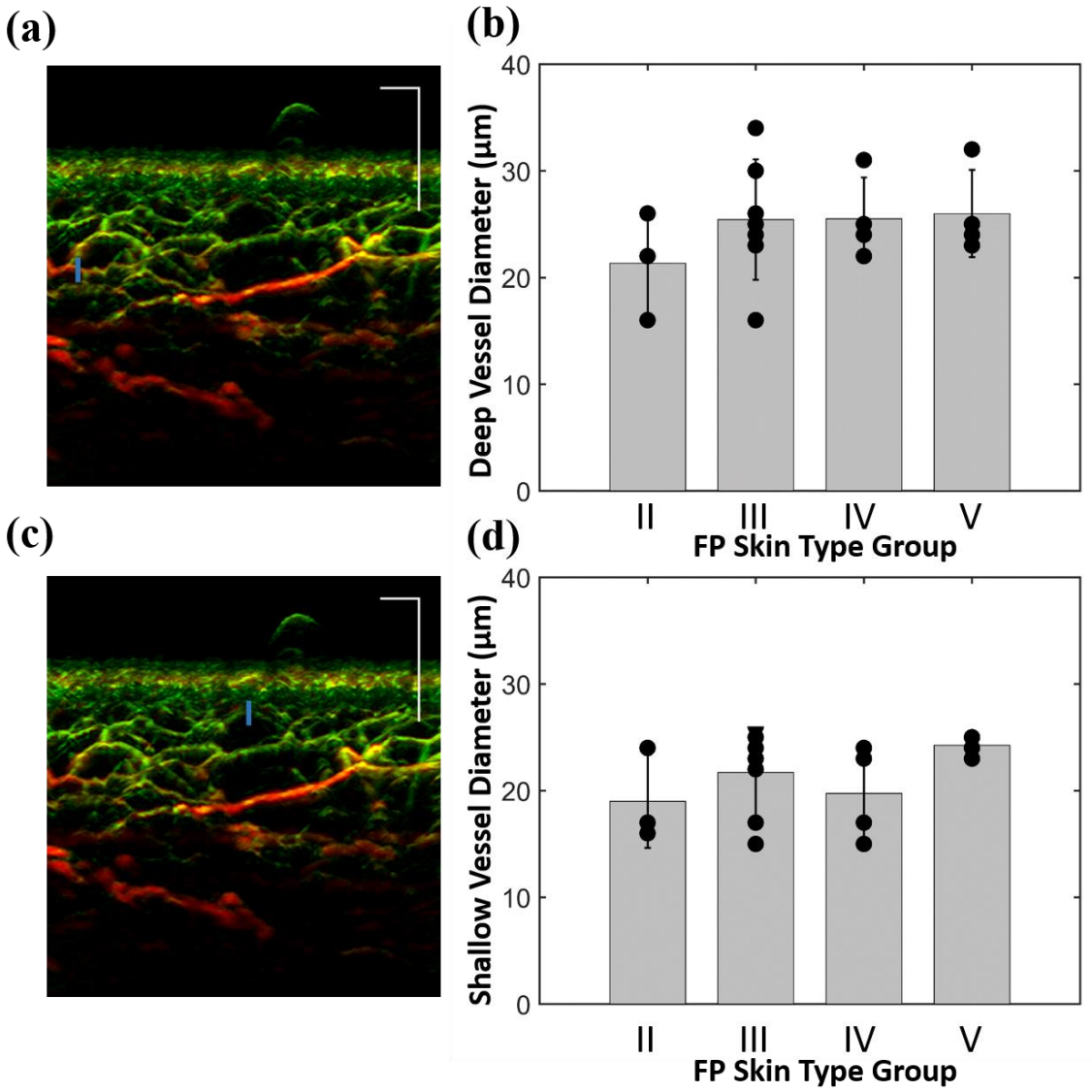

Figure 4. A representative image of a subject of FP type III with the blue lines indicating where the optoacoustic profile was plotted for corresponding selected vessel in the **(a)** deep and **(c)** superficial dermis. All scale bars; 500 μm. The vessel diameter was then calculated as FWHM of the optoacoustic signal. The mean vessel diameter in the vascular plexus of the skin in the **(b)** deep and **(d)** superficial dermis is calculated for each FP skin type. No statistically significant differences were detected (p > 0.05) for the vessel diameters of all FP skin types in both deep and superficial dermis.